



Numerical and experimental investigation of air distribution in a full-scale experimental barn-integrated operating room for general thoracic surgery

Yan Jiang^{1#}, Yongmei Yang^{2#}, Xiaoying Li³, Chao Xu³, Zan Chen², Jianmin Yan⁴, Yanmin Liu³, Xiao Zhou¹

¹Department of Thoracic Surgery, Shanghai Pulmonary Hospital, Tongji University School of Medicine, Shanghai, China; ²Department of Infrastructure Management, Shanghai Pulmonary Hospital, Tongji University School of Medicine, Shanghai, China; ³School of Mechanical Engineering, Tongji University, Shanghai, China; ⁴Shanghai Health Construction Design Institute Co., Ltd, Shanghai, China

Contributions: (I) Conception and design: X Zhou, Y Liu; (II) Administrative support: X Zhou, Y Liu; (III) Provision of study: All authors; (IV) Collection and assembly of data: All authors; (V) Data analysis and interpretation: All authors; (VI) Manuscript writing: All authors. (VII) Final approval of manuscript: All authors.

[#]These authors contributed equally to this work.

Correspondence to: Xiao Zhou. Department of Thoracic Surgery, Shanghai Pulmonary Hospital, Tongji University School of Medicine, Shanghai, China. Email: zx_ty68@163.com; Yanmin Liu. School of Mechanical Engineering, Tongji University, Shanghai, China. Email: liuyanmin@tongji.edu.cn.

Background: Barn-integrated operating rooms have been used in an effort to save space and improve operating room efficiency during orthopedic surgeries. This study aimed to investigate the feasibility of performing several thoracic surgeries in a barn-integrated operating room simultaneously.

Methods: Both numerical simulation and field measurement approaches were applied to evaluate the performance of the ventilation system for the barn-integrated operating room. Computational fluid dynamics (CFD) method was applied to simulate airflow velocity field and particle concentration field. On-site test of airflow velocities were measured with a thermal anemometer. Bacteria-carrying particle (BCP) deposition and distribution was estimated using passive air sampling (PAS) and active air sampling (AAS) methods during mock surgeries.

Results: The airflow distribution and concentration contours showed the barn-integrated operating room to be highly effective in controlling the concentration of airborne bacteria in the operating fields. The airflow and bacteria count met the current standard of GB50333-2013 Specifications, and there was no evidence of air mixing between cabins.

Conclusions: A barn-integrated operating room with several ultraclean operating tables in a single room would be a viable proposition for general thoracic surgeries in the future. As well as achieving a satisfactory level of contamination control, such an approach would reduce operating costs.

Keywords: Barn-integrated operating room; general thoracic surgery; ventilation system; airflow velocity; bacteria-carrying particle (BCP)

Submitted May 12, 2020. Accepted for publication Jun 12, 2020.

doi: 10.21037/atm-20-4349

View this article at: <http://dx.doi.org/10.21037/atm-20-4349>

Introduction

In recent decades, lung cancer has become a critical global health concern affecting an increasing number of people, as well as the leading cause of cancer-related mortality in China (1). In many cases, lung cancer patients

need a surgical operation to remove the tumor. Owing to advances in medical technologies over the last decade, traditional wide-exposure, open surgery has been replaced by minimally invasive thoracic surgery (2). Video-assisted thoracic surgery (VATS) has matured into a reproducible,

Table 1 Wall boundary conditions of personnel and equipment

Personnel and equipment	Quantity	Surface area (m ²)	Heat flux (W/m ²)	Total heat dissipation (W)
Anesthetist	2	2.56	30	154
Surgeon	3	2.56	30	231
Nurse	2	1.71	45	154
Patient	1	1.99	20	60
Anesthesia machine	1	4.48	45	200
Surgical lamp	2	0.75	53	80
Pendant system	2	6.35	31.5	400
Light strip	1	4.2	3.1	13.4

Table 2 Vent configuration

Cleanliness level	Vent classification	Air volume (m ³ /h)	Vent size (mm × mm)	Quantity of vents	Airflow velocity (m/s)
I	Supply vent	9,000	2,600×2,400	1	0.401
	Return vent	3,000 (lower)	1,000×400	2	1.042
		5,000 (upper)	2,000×250	4	0.694
	Exhaust vent	500	360×360	1	1.072
III	Supply vent	3,000	2,600×1,400	1	0.229
	Return vent	2,000 (lower)	1,000×400	2	0.694
		– (upper)	2,000×250	4	–
	Exhaust vent	500	360×360	1	1.072

and III, providing variable air volume depending on the cleanliness demanded by the particular surgical procedure. When all three plenums were switched on at the same time, class I cleanliness was expected to be achieved, with a supply air volume of 9,000 m³/h and section air velocity of 0.4 m/s. When the side plenums were switched off, class III cleanliness was expected, with a supply air volume of 3,000 m³/h and section air velocity of 0.22 m/s.

Numerical model of the velocity field

The velocity field of the model was simulated with CFD software Fluent16.0 (ANSYS Inc., Pennsylvania, USA). Grid dependency tests were carried out to ensure that the results were appropriate and would not vary when the grid density was increased. Grid-independency was achieved by refining the mesh size when the total number of the meshes reached 1.86×10⁶. The human body and equipment were modeled as cuboids to ensure the simplicity of the model.

Table 1 shows the configuration of the vents. All of the interior walls were seen as no slip, and the wall boundary conditions of personnel and equipment are shown in *Table 2*. All sensible heat energy released by surgical personnel and medical equipment was taken as 100% convective and was assumed to be uniform at the emitting surfaces; Chow *et al.* found that such simplification had little bearing on simulation results (6).

The standard k-ε model was employed to simulate airflow. SIMPLE algorithm was applied in the pressure-velocity coupling calculation. In the k-ε model, a second-order upwind difference scheme was used for discretization of the convection terms. Converged solutions were assumed when the summations of residuals were lower than 10⁻⁶ for energy equations and lower than 10⁻⁴ for other equations.

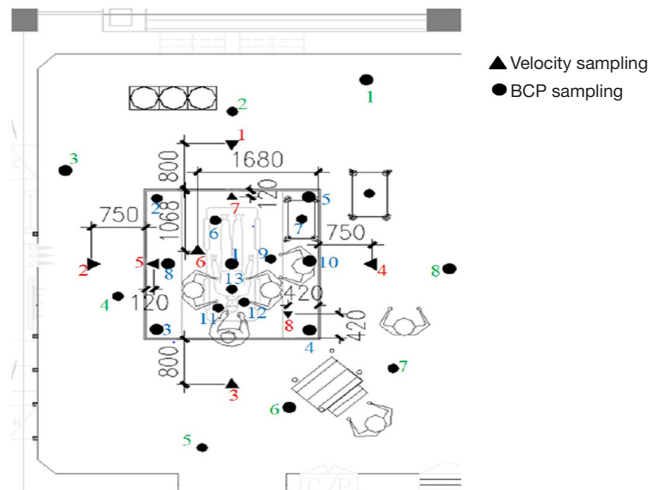
Numerical simulation of particle motion

A Lagrangian-based discrete random walk (DRW) model

Table 3 Bacteria emission of surgical staff members [CFU/(p-min)]

Personnel	Upper body	Lower body
Surgeon	200	400
Nurse	150	350
Anesthetist	200	400

CFU, colony forming units

**Figure 3** Locations of the air velocity and bacteria carrying particle (BCP) sampling points.

was used to simulate the particle concentration field. In our simulation, bacteria-carrying particles (BCPs) were assumed to be $6\ \mu\text{m}$ in diameter and have a material density of $1,000\ \text{kg}/\text{m}^3$ (7). It was assumed that no bacteria was emitted from the patient. The bacteria emission from members of surgical staff members is shown in *Table 3*. The particle boundary conditions were defined as “trap” for the body surface of the patient and the instrument table and surgical table surfaces, “escape” for inlets and outlets, and “reflect” for walls. All contaminant sources were assumed to be uniform at the emitting surfaces.

Field test of airflow velocity

Airflow velocities were measured with a thermal anemometer (TSI Inc., Shoreview, MN), which is a unidirectional air velocity transducer with a range of 0.13–50 m/s and a reading accuracy of $\pm 2\%$. The uniformity of the air velocity was checked by taking measurements at 15 cm underneath the plenums. Data were collected once

per second. *Figure 3* shows the locations of the air velocity collection points.

Bacteriological air sampling

Field tests of particle counts and microbial counts were conducted during mock surgeries. Samples were taken from the positions shown in *Figure 3*. The deposition and distribution of BCPs in the operating room were estimated using the passive air sampling (PAS) and active air sampling (AAS) methods. For PAS, nutrient agar plates were exposed to the air for 0.5 h. BCPs were impacted onto the surface of the nutrient agar plates and then incubated for 24 h at $37\ ^\circ\text{C}$. For AAS, the air was sampled using a slit sampler working at 40 L/min for 8 min, and then directed toward the surface of nutrient agar plates, followed by incubation in $37\ ^\circ\text{C}$ for 24 h. The number of colony forming units (CFU) was counted to establish the number of aerobic bacteria/ m^3 in the air.

Results

Simulated velocity distribution under class I and III operating room setting

Figure 4 displays the CFD predicted airflow pattern under the class I operating room setting. As shown in *Figure 4A* and *B*, the surgical lamps influenced the airflow above the operating table considerably, leading to turbulence underneath the surgical lamps. The flow velocity in the region below the medical lamps dropped, and the unidirectional airflow diminished locally, while the streamlines were basically parallel in the area away from the surgical light. As *Figure 4C* shows, there was a degree of air turbulence in the clean corridor; nonetheless, this occurrence had a negligible effect on the air flow in the critical surgical region, which remained relatively uniform due to the large volume of supply air. The air velocity at the centerline of the operating table decreased from 0.45 to 0.125 m/s above the waist of the patient, because of a thermal plume caused by heat dissipation from the surgical personnel and medical equipment. Nevertheless, the clean air from the main air supply device continued to exhibit a good washing effect in the vicinity of the patient's chest (the wound site). As shown in *Figure 4D*, upper return air velocity was large enough to form an air curtain between the two cabins, while no re-entrainment, which can cause clean air to become contaminated, occurred. Thus, the

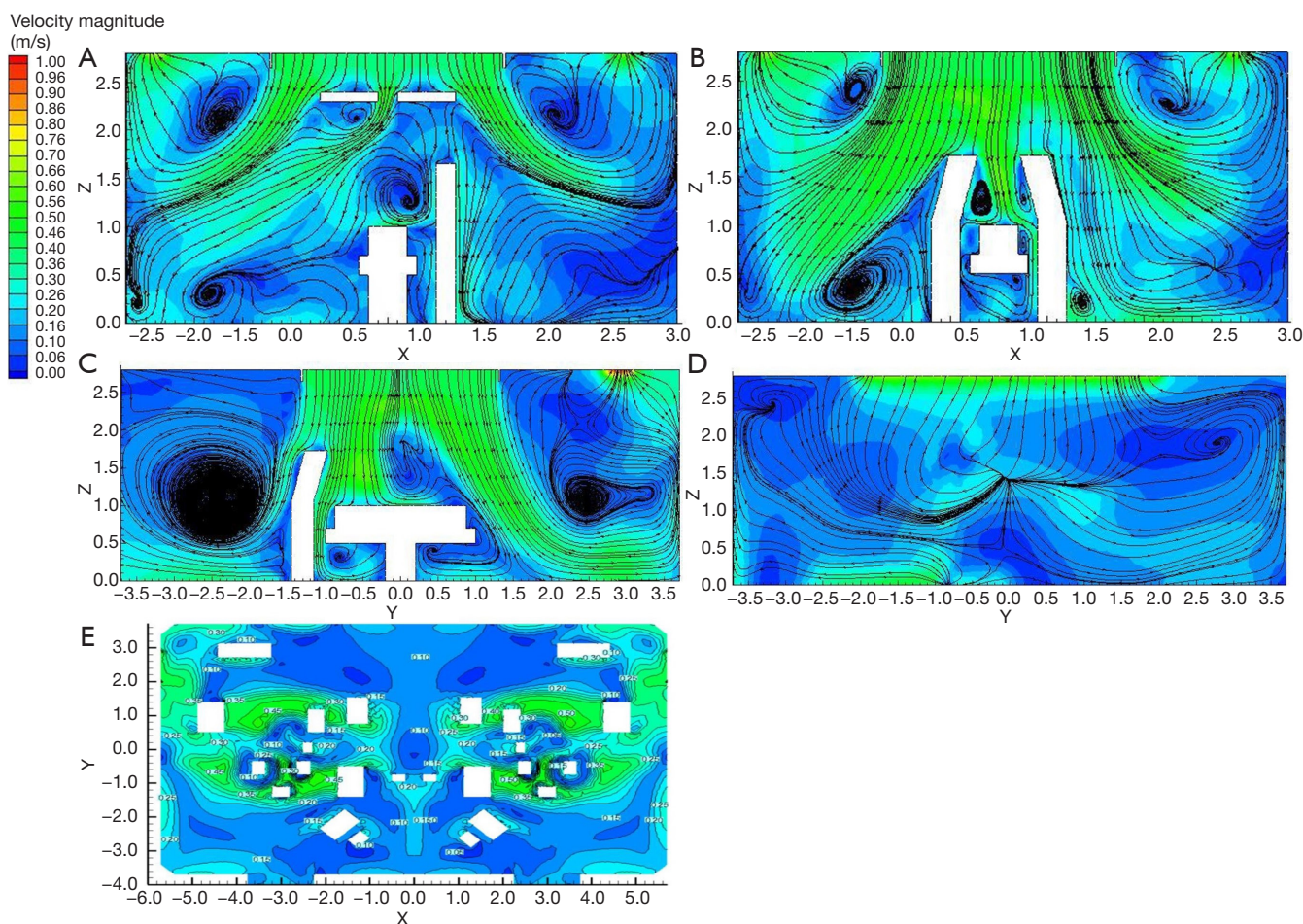


Figure 4 Velocity magnitude contours showing airflow patterns in the class I operating room. (A) Simulated airflow velocity at the vertical plane of $Y=0$ m; (B) simulated airflow velocity at the vertical plane of $Y=-0.45$ m; (C) simulated airflow velocity at the vertical plane of $X=0$ m; (D) simulated airflow velocity at the plane passing through the centerline of upper return vent; (E) simulated airflow velocity at the horizontal plane of $Z=1.2$ m.

clean supply air to above the operating area was delivered directly and smoothly. *Figure 4E* shows the velocity field at the horizontal section of $Z=1.2$ m, which covered a large area of high-velocity above the surgical site, with the air velocity at its perimeter region approaching 0.35 m/s. A velocity separation zone was formed in the shared region between the two cabins, which was conducive to avoiding mutual interference between the two surgical areas.

Figure 5 reflects the velocity distribution under a class III operating room setting. As shown in *Figure 5A* and *B*, a zone of low velocity beneath the surgical lamp and turbulence existed, while the airflow streamline in the area not obstructed by the operating lamp basically remained parallel, with the maximum flow rate approaching 0.4 m/s.

Turbulence existed on the clean corridor side (*Figure 5C*). Due to the heat dissipation from the patient, the airflow above the patient decreased slightly, with the air velocity reaching the body surface of the patient at about 0.2 m/s. The air velocity in the surgical area was well above 0.2 m/s, which effectively prevented the interference of airflow from the adjacent area (*Figure 5D*).

BCP concentration

Figure 6 shows the particle concentration contours for different sections in a class I operating room. As shown by *Figure 6A* and *B*, a stagnant area with a high concentration of BCP developed underneath the surgical lamps, owing

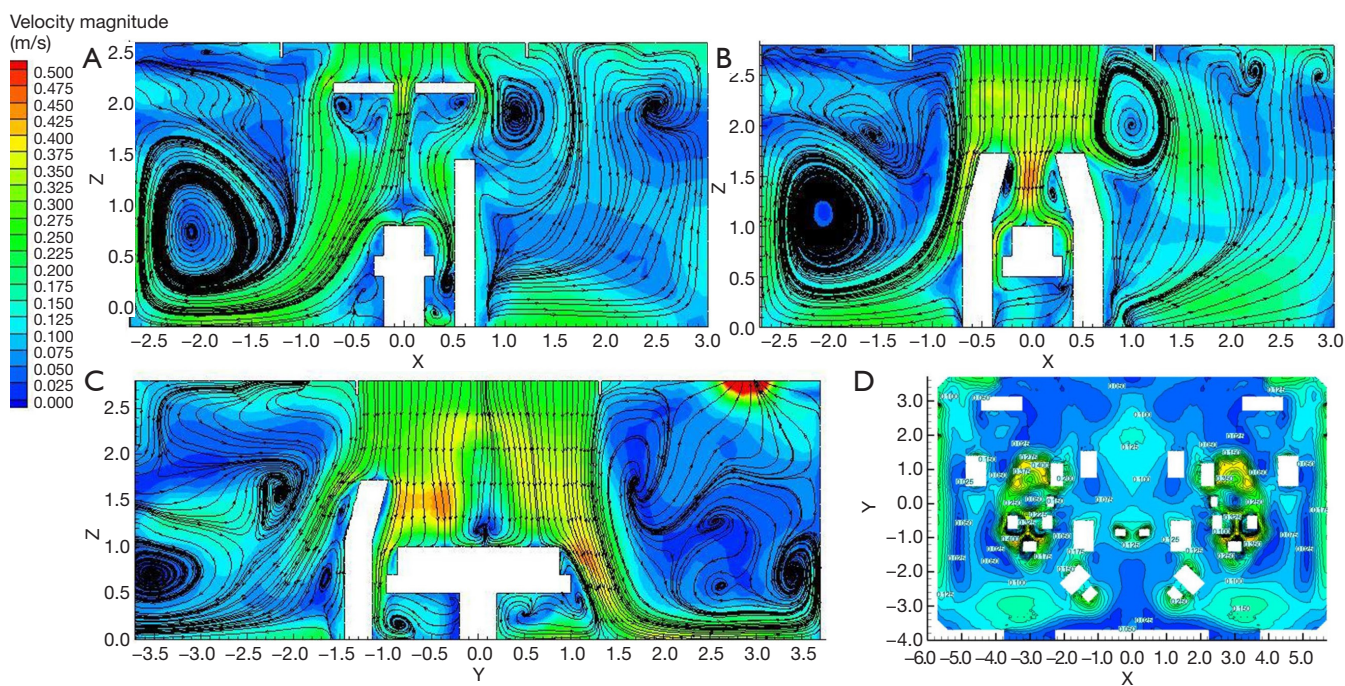


Figure 5 Velocity magnitude contours showing airflow patterns in the class III operating room. (A) Simulated airflow velocity at the vertical plane of $Y=0$ m; (B) simulated airflow velocity at the vertical plane of $Y=-0.45$ m; (C) simulated airflow velocity at the vertical plane of $X=0$ m; (D) simulated airflow velocity at the horizontal plane of $Z=1.2$ m.

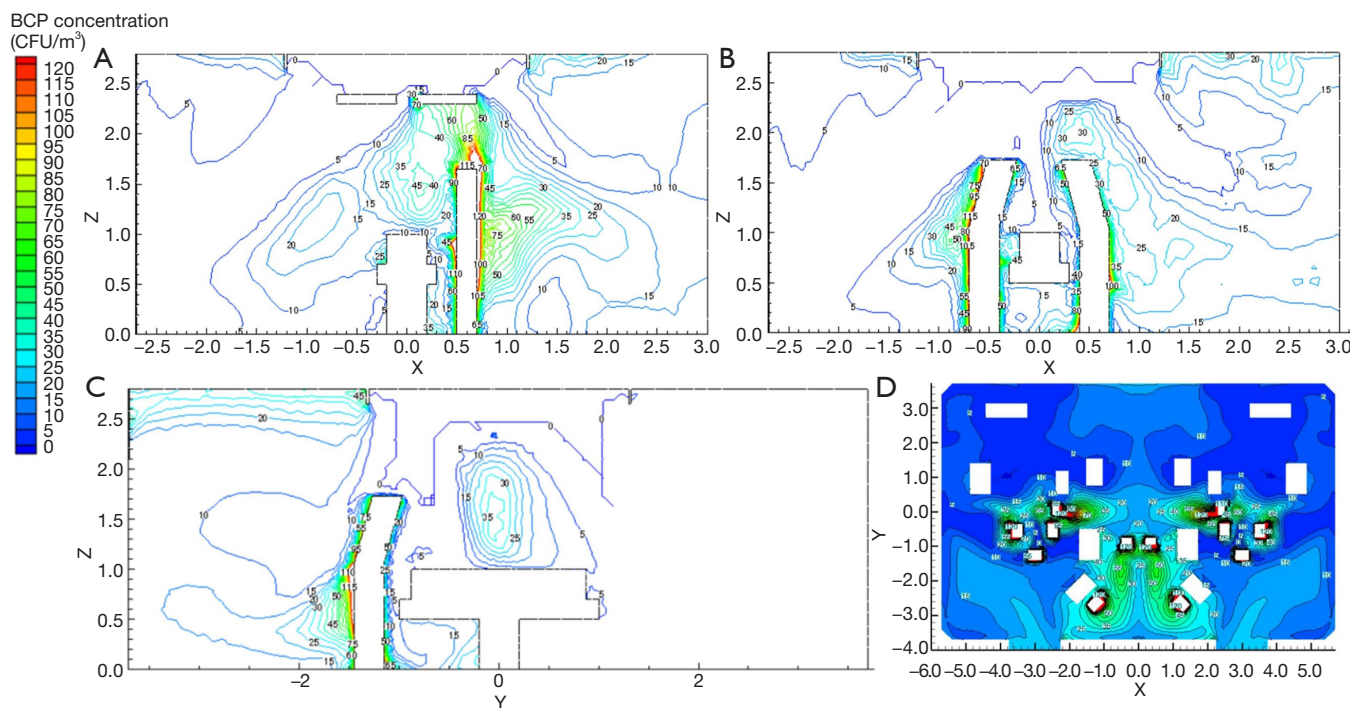


Figure 6 Concentration contours showing bacteria carrying particle (BCP) concentration in the class I operating room. (A) Simulated BCP concentration at the vertical plane of $Y=0$ m; (B) simulated BCP concentration at the vertical plane of $Y=-0.45$ m; (C) simulated BCP concentration at the vertical plane of $X=0$ m; (D) simulated BCP concentration at the horizontal plane of $Z=1.2$ m.

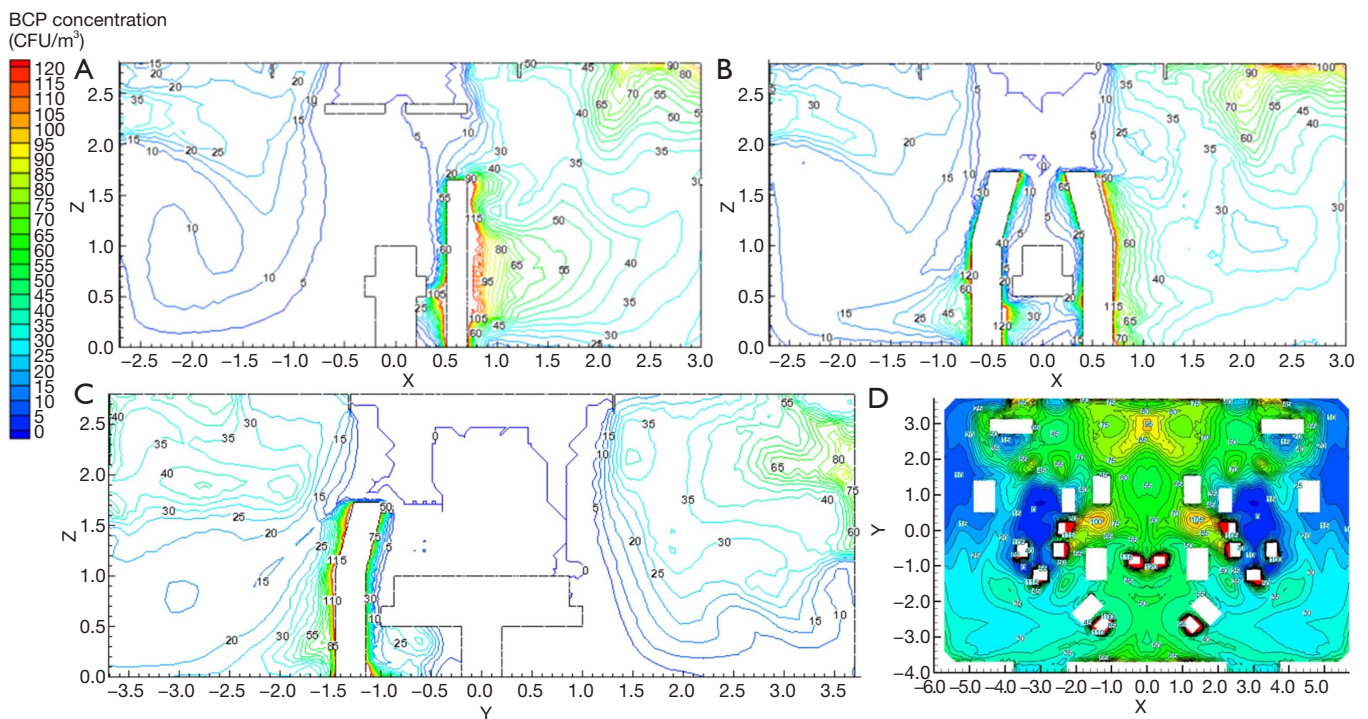


Figure 7 Concentration contours showing bacteria carrying particle (BCP) concentration in the class III operating room. (A) Simulated BCP concentration at the vertical plane of $Y=0$ m; (B) simulated BCP concentration at the vertical plane of $Y=-0.45$ m; (C) simulated BCP concentration at the vertical plane of $X=0$ m; (D) simulated BCP concentration at the horizontal plane of $Z=1.2$ m.

to its close vicinity to sources of contamination, such as the surgeons, and the obstruction of airflow by the surgical lamps. The BCP concentration at the waist of the patient reached 10 CFU/m^3 . However, at the chest of the patient, it was reduced to 5 CFU/m^3 , which indicated a fast decay rate of the pollutant particles. Despite the existence of a region with BCP concentration of $10\text{--}35\text{ CFU/m}^3$ caused by heat dissipation from medical personnel and the obstructive effect of the surgical lamps, the high pollutant concentration area was not in the vicinity of the patient's body surface (Figure 6C). The concentration of infectious particles near the patient's body surface was reduced to 5 CFU/m^3 , which met the specification of a class I operating room. Meanwhile, the particle concentration at the front side of the operating room was significantly higher than that at the back side, due to the lack of exhaust and return air outlets in the front, which generated turbulence in the clean corridor and led to particle retention (Figure 6D). The BCP concentration on the exhaust corridor side was much lower, as the polluted air was discharged smoothly. The concentration of pollutants near the medical personnel was high, since the skin squames emitted by the medical personnel were the main source of

pollution (7). Nevertheless, the decay rate was high, and the concentration of infectious particles in the vicinity of the patient was reduced to 5 CFU/m^3 , which indicated an effective washing effect of the airflow.

Figure 7 shows the particle concentration contours for different sections of the class III operating room. Figure 7A shows that the BCP concentration on the left side of the operating room was significantly lower than that of the right side, because there were fewer sources of pollution on the left side. As shown in Figure 7B, the clean air was delivered directly to the key surgical area without the obstruction of surgical lamps; thus, the pollutant concentration was extremely low and met the requirements of the specification. Clean air from the canopy was delivered directly into the surgical area with no obstacles (Figure 7C), and the airflow covered the surgical area entirely. As a result, the pollutant concentration was much lower than the specification of 75 CFU/m^3 . While the pollutant concentration in the surrounding area was relatively higher, it still met requirements of the specification of 100 CFU/m^3 . Moreover, despite the relatively high BCP concentration in the exhaust corridor, the concentration of pollutants was

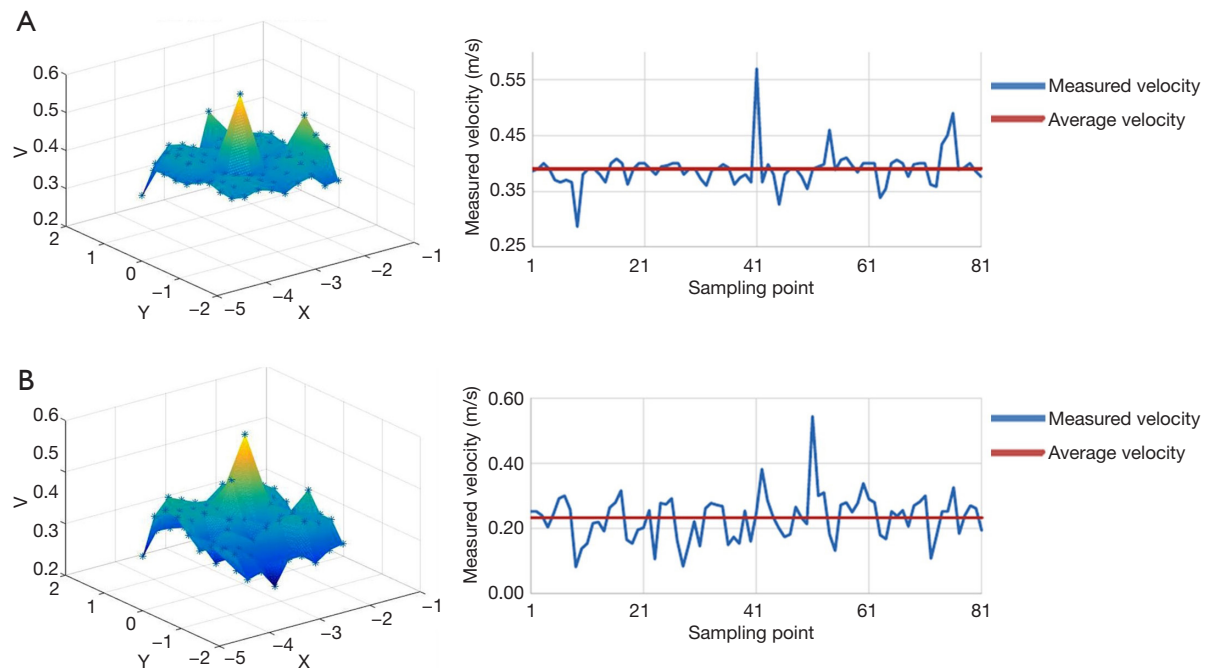


Figure 8 The measured airflow velocity in the class I operating room in a static state. (A) Airflow velocity at the horizontal plane of $Z=2.7$ m; (B) airflow velocity at the horizontal plane of $Z=1.2$ m.

low on the clean corridor side (Figure 7D).

In situ assessment of air flow velocities

Airflow velocities were measured with a thermal anemometer at 1.2 m from the floor of the surgical site. Air velocities under the canopy were measured in a static or dynamic state. Before each test, the uniformity of the air velocity of the canopies was tested, and the airflow velocities were conducted within 5% deviation from the designed value of 0.40 m/s. In the right cabin, the average air velocity of the canopy was 0.41 m/s, with a deviation of 2.5% from the designed value. Figure 8 shows the measured airflow velocity under a class I operating room setting in a static state. The average air velocity of the whole plane at a height of 2.7 m was 0.39 m/s, with a deviation of 2.5% from the designed value of 0.40 m/s. At a height of 1.2 m, the average velocity of the plane was 0.233 m/s with a deviation of 7.6%, which met the requirements of 0.20–0.25 m/s. Notably, a maximum air velocity of 0.544 m/s caused by the gap between the two surgical lamps was observed.

Figure 9 displays the measured airflow velocity of a class I operating room in a dynamic state. The mean measured air velocity at heights of 2.7 and 1.2 m was 0.39 and

0.232 m/s, respectively, which met the requirements of 0.20–0.25 m/s in the specification.

In situ assessment of BCP concentration

Table 4 shows the concentration of BCPs captured by the slit samplers or settled over the agar plates. Bacterial counts by AAS and PAS at the surgical site and surrounding area were extremely low and well within the current standard recommended in GB50333-2013 (8). The desired concentration of <10 CFU/m³ for infection-sensitive surgery was achieved.

Discussion

In this study, the feasibility of introducing barn-integrated operating room to general thoracic surgery was investigated. The airflow pattern and BCP concentration in the experimental barn-integrated operating room were explored both numerically and physically. The simulated and tested airflow pattern and BCP concentration in the barn-integrated operating room were generally satisfactory and met the standards described in GB50333-2013, and there was no evidence of air from one unit mixing with air

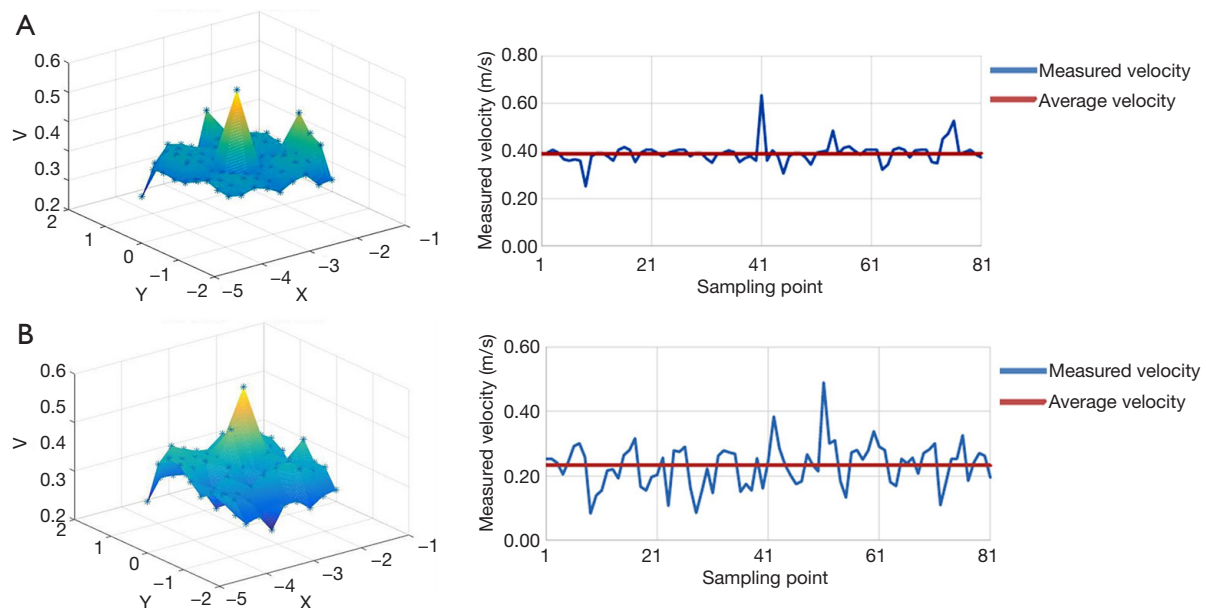


Figure 9 The measured airflow velocity in the class I operating room in a dynamic state. (A) Airflow velocity at the horizontal plane of $Z=2.7$ m; (B) airflow velocity at the horizontal plane of $Z=1.2$ m.

Table 4 Concentration of infectious particles (CFU/m^3)

Method	Area	Measured concentration	Required concentration
PAS	Surgical site	0.2	0.2
	Surrounding site	0.4	0.4
AAS	Surgical site	0.6	5
	Surrounding site	1.2	10

CFU, colony forming units

from another.

Barn-integrated operating rooms enable several operations to be performed simultaneously. Moreover, they ensure optimum use of operating room capacity by facilitating the sharing of support services, and if necessary, they can provide sufficient space to accommodate the surgical team and larger items of mobile equipment. These benefits offer solutions for the ever-increasing demand for surgeries.

Importantly, the cleanliness level of the operating room could be adjusted flexibly depending on the particular surgery to be performed. For certain types of surgery during which the risks of airborne spread are low, such as minimally invasive surgery, the ventilation system would be set to class III. Meanwhile, for surgeries with high risk

of airborne infection, like lung transplantation surgery, the ventilation system would be adjusted to class I. In this way, substantial amounts of energy and running costs would be saved, while the demands of infection control could be met.

One major limitation of the present study was that the airflow velocity and BCP concentration measurements did not include the presence of real surgical staff, which was mimicked by the presence of thermal dummies. Since the airflow velocity distribution and BCP concentration above the surgical bed would be influenced by the movement of surgeons and the thermal plume generated by them and the patient, these results should be carefully interpreted (9,10). Therefore, the infection rate cannot be predicted at this stage. Further investigation is needed to generate the most appropriate design of ventilation systems for the use of barn-integrated operating rooms in thoracic surgery.

Conclusions

The present study demonstrated that barn-integrated operating room, which has historically been used for orthopedic surgeries, is feasible for use for general thoracic surgeries in the future. The barn-integrated operating room can offer the ideal operating situation in an energy-efficient manner, with the potential for efficient space utilization and improved training opportunities for junior

surgeons and anesthetists, as well as reduced infection rates. It is envisaged that barn-integrated operating room will bring about substantial change to the way surgery is managed, by providing an enhanced service and improved patient flow.

Acknowledgments

Funding: This work was supported by the China National Key R&D Program “Energy-saving design and key technical equipment development for clean air-conditioning plants” (Grant No. 2018YFC0705205).

Footnote

Data Sharing Statement: Available at <http://dx.doi.org/10.21037/atm-20-4349>

Conflicts of Interest: All authors have completed the ICMJE uniform disclosure form (available at <http://dx.doi.org/10.21037/atm-20-4349>). The authors have no conflicts of interest to declare.

Ethical Statement: The authors are accountable for all aspects of the work in ensuring that questions related to the accuracy or integrity of any part of the work are appropriately investigated and resolved.

Open Access Statement: This is an Open Access article distributed in accordance with the Creative Commons Attribution-NonCommercial-NoDerivs 4.0 International License (CC BY-NC-ND 4.0), which permits the non-commercial replication and distribution of the article with the strict proviso that no changes or edits are made and the original work is properly cited (including links to both the formal publication through the relevant DOI and the license). See: <https://creativecommons.org/licenses/by-nc-nd/4.0/>.

Cite this article as: Jiang Y, Yang Y, Li X, Xu C, Chen Z, Yan J, Liu Y, Zhou X. Numerical and experimental investigation of air distribution in a full-scale experimental barn-integrated operating room for general thoracic surgery. *Ann Transl Med* 2020;8(12):759. doi: 10.21037/atm-20-4349

References

1. Bray F, Ferlay J, Soerjomataram I, et al. Global cancer statistics 2018: GLOBOCAN estimates of incidence and mortality worldwide for 36 cancers in 185 countries. *CA Cancer J Clin* 2018;68:394-424.
2. Guido-Guerrero W, Bolaños-Cubillo A, et al. Single-port video-assisted thoracic surgery (VATS)—advanced procedures & update. *J Thorac Dis* 2018;10:S1652-61.
3. Donnelly J, Greaves J. 'The Barn'. *Br J Theatre Nurs* 1991;1:4-5.
4. Babb JR, Lynam P, Ayliffe GA. Risk of airborne transmission in an operating theatre containing four ultraclean air units. *J Hosp Infect* 1995;31:159-68.
5. Liu Y, Li X, Yan J, et al. Evaluation and optimization for solid models of barn integrated operating room. *Journal of Chinese Hospital Architecture & Equipment* 2018;19:39-44.
6. Chow TT, Lin Z, Bai W. The integrated effect of medical lamp position and diffuser discharge velocity on ultra-clean ventilation performance in an operating theatre. *Indoor and Built Environment* 2006;15:315-31.
7. Zhang R, Tu G, Ling J. Study on biological contaminant control strategies under different ventilation models in hospital operating room. *Building and Environment* 2008;43:793-803.
8. MOUHRD of the PRC. GB 50333-2013 Architectural technical code for hospital clean operating department. Beijing: China Architecture and Building Press, 2013.
9. Aganovic A, Cao G, Stenstad LI, et al. Impact of surgical lights on the velocity distribution and airborne contamination level in an operating room with laminar airflow system. *Building and Environment* 2017;126:42-53.
10. Chow TT, Wang JL. Dynamic simulation on impact of surgeon bending movement on bacteria-carrying particles distribution in operating theatre. *Building and Environment* 2012;57:68-80.